# Macromolecules

# Morphology and Proton Transport in Humidified Phosphonated Peptoid Block Copolymers

Jing Sun,[†,⊥] Xi Jiang,[‡] Aaron Siegmund,[#] Michael D. Connolly,[†,‡] Kenneth H. Downing,[§] Nitash P. Balsara,[*,‡,∥,%] and Ronald N. Zuckermann[*,†,‡]

[†]Molecular Foundry, [‡]Materials Sciences Division, [§]Molecular Biophysics and Integrated Bioimaging Division, [∥]Environmental Energy Technologies Division, Lawrence Berkeley National Laboratory, Berkeley, California 94720, United States
[⊥]School of Polymer Science and Engineering, Qingdao University of Science and Technology, Qingdao, China 266042
[#]Department of Medicinal Chemistry, Amgen Inc., One Amgen Center Drive, Thousand Oaks, California 91320-1799, United States
[%]Department of Chemical and Biomolecular Engineering, University of California, Berkeley, California 94720, United States

**S** *Supporting Information*

**ABSTRACT:** Polymers that conduct protons in the hydrated state are of crucial importance in a wide variety of clean energy applications such as hydrogen fuel cells and artificial photosynthesis. Phosphonated and sulfonated polymers are known to conduct protons at low water content. In this paper, we report on the synthesis phosphonated peptoid diblock copolymers, poly-*N*-(2-ethyl)hexylglycine-*block*-poly-*N*-phosphonomethylglycine (pNeh-*b*-pNpm), with volume fractions of pNpm ($\phi_{Npm}$) values ranging from 0.13 to 0.44 and dispersity ($Đ$) ≤ 1.0003. The morphologies of the dry block copolypeptoids were determined by transmission electron microscopy and in both the dry and hydrated states by synchrotron small-angle X-ray scattering. Dry samples with $\phi_{Npm}$ > 0.13 exhibited a lamellar morphology. Upon hydration, the lowest molecular weight sample transitioned to a hexagonally packed cylinder morphology, while the others maintained their dry morphologies. Water uptake of all of the ordered samples was 8.1 ± 1.1 water molecules per phosphonate group. In spite of this, the proton conductivity of the ordered pNeh-*b*-pNpm copolymers ranged from 0.002 to 0.008 S/cm. We demonstrate that proton conductivity is maximized in high molecular weight, symmetric pNeh-*b*-pNpm copolymers.
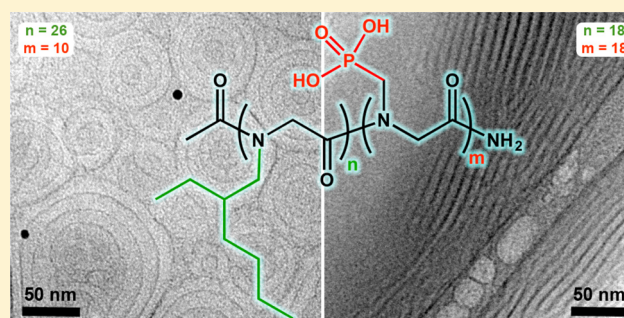
## INTRODUCTION

Proton-conducting polymers have attracted considerable attention because they play a central role as electrolyte membranes in hydrogen fuel cells and artificial photosynthesis.[1−3] The most widely studied membranes are based on sulfonated polymers such as Nafion.[4,5] Nafion is a semicrystalline random copolymer of hydrophobic tetrafluoroethylene and hydrophilic perfluoroether side chains that have terminal sulfonic acid groups. In the dry state, the ionic groups are sequestered in clusters in a hydrophobic tetrafluoroethylene-rich matrix, and Nafion is an insulator. In the wet state, a percolating network of hydrated channels emerges within the hydrophobic matrix by self-assembly, resulting in a mechanically robust proton conducting material. Although numerous papers have been written on this transformation,[6−20] there is still considerable debate surrounding the nanoscale morphology of the hydrated channels. Several groups have embarked on studies of block copolymers comprising a sulfonated block that enables proton conduction and a hydrophobic block that provides the membrane with mechanical integrity.[21−26] The morphology of the conducting channels in these systems can be

readily determined by scattering techniques (either X-ray or neutron scattering) or electron microscopy.

During typical application conditions, polymer electrolyte membranes are exposed to air, and thus the extent of hydration of the membrane is determined by the partitioning of water between the membrane and the surrounding gas phase. As a result, sulfonic acid-based membranes are ineffective proton transporters at high temperatures (above 80 °C), since very little water is retained at high temperatures.[27−30] This limitation has motivated studies of polymers functionalized with other acidic or protogenic groups.[31−33] Phosphonated polymers are attractive systems for several reasons. First, they exhibit efficient proton transport under low water uptake conditions. This is attributed to a higher degree of hydrogen bonding which promotes proton transport by the Grothuss mechanism.[34] Second, the phosphonic acid group can release two protons instead of one because phosphonate are dibasic as compared to sulfonates which are monobasic. Third, phosphonated poly-

mers often show higher chemical and thermal stability, relative to sulfonic acid moieties, in part due to their higher $pK_a$'s.[33] In spite of these advantages, relatively few studies of phosphonated polymers have been reported.[35] This is likely because there are no convenient synthetic routes to phosphonated polymers. In fact, all of the studies of proton transport in phosphonated polymer systems have been restricted to random copolymers. While proton conductivities ranging from $10^{-6}$ to $10^{-1}$ S/cm have been reported for such copolymers,[17] the relationship between morphology and conductivity has not yet been explored.

Herein we report the synthesis and characterization of a family of well-defined phosphonate diblock copolymers: poly-*N*-(2-ethyl)hexylglycine-*block*-poly-*N*-phosphonomethylglycine (pNeh-*b*-pNpm). Polypeptoids are a family of comb-like polymers based on an N-substituted glycine backbone.[36,37] Iterative solid-phase synthesis enables the efficient synthesis of polymers with precise control over chain length and copolymer composition.[38−40] The dispersity of the copolymers (Đ) was less than 1.0003. Microphase separation and hydration results in the formation of pNpm-rich domains that conduct protons in the hydrated state. Here we study the relationship between morphology and proton transport for a family of diblocks containing varying volume fractions of each block.

## ■ EXPERIMENTAL SECTION

**Synthesis of Monomers.** *Di-tert-butyl(phthalimidomethyl)-phosphonate.* In a round-bottom flask, 17.5 g of potassium bis(trimethylsilyl)amide (88 mmol) was suspended in 200 mL of anhydrous tetrahydrofuran (THF) and cooled to −40 °C. 17 g of di-*tert*-butyl phosphite (88 mmol) was added over 20 min. After addition, the flask was warmed to 0 °C and stirred for 30 min. The solution was cooled to −40 °C, and 21 g of *N*-(bromomethyl)phthalimide (Aldrich) in 150 mL of anhydrous THF was added dropwise. After addition, the flask was warmed to room temperature and stirred for 1 h. The solvent was removed under vacuum. The residue was partitioned between 1 L of ethyl acetate and 100 mL of water. The organic layer was washed with water (100 mL), saturated aqueous sodium bicarbonate (100 mL), and brine (100 mL), dried over sodium sulfate, filtered, and concentrated to give an oily solid (32.2 g). The solid was purified by flash chromatography (60 hexanes/39.9 ethyl acetate/0.1 triethylamine), resulting in 19 g (65%) of a white solid. ^{1}H NMR (500 MHz, CDCl$_3$): $d$ = 7.89 (t, 2H, CH=CH−CH), 7.75 (d, 2H, C=CH−CH), 4.03 (d, $J$ = 10, 2H, N−CH$_2$−P), 1.55 (s, 18H, C−(CH$_3$)$_3$).

*Di-tert-butyl(aminomethyl)phosphonate.* The di-*tert*-butyl-(phthalimidomethyl)phosphonate (19 g, 54 mmol) was dissolved in 200 mL of absolute ethanol. Methylhydrazine (9.9 g, 215 mmol) was added dropwise, and the solution was stirred overnight. The solution was concentrated in vacuum, and 250 mL of dichloromethane (DCM) was added. The white solid was removed by filtration and rinsed two times with DCM (100 mL). The filtrate was washed with water (5 × 75 mL) and brine (75 mL), dried over sodium sulfate, and concentrated to yield 11.9 g (99%) of pale yellow oil. ^{1}H NMR (500 MHz, CDCl$_3$): $\delta$ = 2.88 (d, $J$ = 10, 2H, NH$_2$−CH$_2$−P), 1.54 (s, 18H, C−(CH$_3$)$_3$).

**Synthesis of Peptoid Polymers.** Polypeptoids were synthesized on an automated robotic synthesizer or a commercial Aapptec Apex 396 robotic synthesizer on 100 mg of Rink amide polystyrene resin (0.61 mmol/g, Novabiochem, San Diego, CA). The protected phosphonate submonomer, di-*tert*-butyl(aminomethyl)phosphonate, was synthesized by a modification of previously reported methods.[41,42] All the other monomers, solvents, and reagents described here were purchased from commercial sources and used without further purification. The 2-ethyl-1-hexylamine submonomer was used as the racemic mixture. Peptoids were synthesized by a slightly modified version of the solid-phase submonomer method previously

described.[40,43] The Fmoc group on the resin was deprotected with 20% (v/v) 4-methylpiperidine/DMF before starting the monomer cycle. An acylation step was then performed on the amino resin by the addition of 1.0 mL of 1.2 M bromoacetic acid in DMF and 0.18 mL of *N,N′*-diisopropylcarbodiimide (DIC, 1.15 mmol, neat) and mixing for 20 min. Displacement of the bromide with various monomers occurred by adding a 1.0−2.0 M solution of the primary amine in *N*-methyl-2-pyrrolidone, followed by agitation for 120 min. All the polymers were acetylated on the resin after synthesis using a mixture (2.0 mL per 100 mg of resin) of 0.4 M acetic anhydride and 0.4 M pyridine in DMF for 30 min. The crude peptoid products were cleaved from the resin by the addition of 95% (v/v) trifluoracetic acid (TFA) in H$_2$O for 1 h, followed by evaporation. The crude products were then directly precipitated from water. The final polypeptoids were then lyophilized prior to subsequent measurements.

The molecular weight of each final product was characterized by electrospray ionization (ESI) mass spectrum from a solution (50 mM in methanol), containing a trace of triethylamine. The molecular weight of the polypeptoid pNeh$_9$-*b*-pNpm$_9$ was determined by matrix-assisted laser desorption/ionization mass spectrometry (Applied Biosystems MALDI TOF/TOF Analyzer 4800) with a 1:1 (v/v) mixture of peptoid [2 mg/mL in 1:1 (50:50 THF:methanol):water] and α-cyano-4-hydroxycinnamic acid dissolved in THF at saturated concentration.

All polymers were characterized by ^{1}H NMR (500 MHz, CD$_3$OD), shown in Figure S2. The peaks marked with b (at 4.4 ppm, NCH$_2$CO in pNeh), a (at 4.2 ppm, NCH$_2$CO in pNpm), c (at 3.3 ppm, NCH$_2$CH), and d (at 3.9 ppm, NCH$_2$P) are assigned to the protons of the pNeh and pNpm blocks. The peaks e−j (at 0.9−1.8 ppm) can be assigned to the protons of the alkyl group in the pNeh blocks.

**Density Measurement.** The density of polypeptoids was measured using a density gradient column with a sucrose solution at room temperature as previously described.[44] An aqueous sucrose gradient was used in the density gradient column method. The measured density was used to calculate the volume fraction of the polypeptoids. The densities of pNpm and pNte were measured to be $1.13 \pm 0.01$ and $1.23 \pm 0.01$ g/cm$^3$.

**Differential Scanning Calorimetry (DSC).** Differential scanning calorimetry (DSC) experiments were performed to determine the thermal behavior of the synthesized peptoids using a TA Q200 differential scanning calorimeter. In all tests, a scan rate of 10 K/min was used in the temperature range of −20 to 200 °C for three heating and cooling cycles.

**Thermogravimetric Analysis (TGA).** Samples were characterized using a TA Instruments TGA to investigate degradation temperatures by mass loss. Approximately 5.0 mg of lyophilized peptoid powder was placed on an aluminum sample pan. Samples were equilibrated at 30 °C for 20 min and then heated to 500 °C at 5 °C/min under a nitrogen atmosphere.

**Water Uptake.** Water uptake of pNeh-*b*-pNpm equilibrated in humid air was measured in a humidity-controlled environmental chamber (SH-241, Espec. Corp). A small piece of water-equilibrated sample was placed in a quartz pan which was hooked on the end of a quartz spring (Deerslayer) in the humidity chamber. Samples were equilibrated at the humidity level of interest for 12 h before measurements were recorded. The weight of the wet sample, $W_{wet}$, was obtained by measuring spring length through a port on the wall of the humidity chamber by a cathetometer equipped with an optical zoom telescope located outside the chamber. Care was taken to minimize the time when the port was opened (typically 10 s). The spring was calibrated with standard masses at experimental temperatures and relative humidity in the chamber before use (spring constant was about 0.5 mN/mm). The sample pellet was dried in vacuum at 40 °C for 24 h. It was allowed to cool down in a desiccator before the dry sample weight, $W_{dry}$, was measured. Water uptake is given by eq 1.

$$\text{water uptake} = (W_{\text{wet}} - W_{\text{dry}})/W_{\text{dry}} \times 100\% \tag{1}$$

The ion exchange capacity (IEC) and the number of water molecules per phosphoric acid group (hydration number), $\lambda$, were calculated from water uptake:

$$\text{IEC (mmol/g)} = 10^3 m/(169 \times n + 151 \times m + 59) \quad (2)$$

$$\lambda = \text{water uptake (\%)} \times 10/(\text{MW}_{H_2O} \times \text{IEC}) \quad (3)$$

where $\text{MW}_{H_2O}$ = 18.02 g/mol.

**Small/Wide-Angle X-ray Scattering (SAXS/WAXS).** The block copolypeptoid was dissolved in a 1:1 (v/v) mixture of methanol and tetrahydrofuran and stirred overnight. The solution was then cast on ultraclean Kapton film on a custom-built solvent caster maintained at 35 °C, using a doctor blade. The concentration of the solution and the height of the doctor blade were adjusted to obtain a membrane with a thickness of ~120 $\mu$m. The membrane was dried under vacuum overnight, annealed at relative humidity (RH) = 98%, and dried again before measurements. All of these steps were carried out at room temperature. Because of the lack of access to a humidity-controlled chamber appropriate for SAXS experiments, wet samples were prepared by placing the cast samples (with the Kapton substrate) in a closed SAXS sample stage containing water. Samples were equilibrated for 2 h before measurements were taken. Synchrotron SAXS was performed at beamline 7.3.3 at the Advanced Light Source (ALS) at Lawrence Berkeley National Laboratory (LBNL). A silver behenate sample was used as a standard. Full two-dimensional scattering patterns were collected on an ADSC CCD detector. The scattering patterns from ALS were reduced using the Nika program for Igor Pro available from Jan Ilavsky at Argonne National Laboratory.[45]

**Transmission Electron Microscopy (TEM).** Ultrathin films of peptoid diblock copolymers were prepared by drop casting 0.1 wt % MeOH/THF 50:50 solutions on the gold grids that covered by lacey carbon supporting films. All grids were annealed in the same humidity chamber described above at 25 °C, relative humidity 98% for 24 h. The annealed films were dried either partially by storing them stored in air (35% humidity) or fully under ultrahigh vacuum (lower than $10^{-7}$ Torr) in the transmission electron microscope column. Samples were imaged without any staining using both energy filtered transmission electron microscopy (EFTEM) at a 200 kV acceleration voltage with a slit width of 20 eV on a Tecnai F20 (FEI Company. Netherlands). The thickness of the ultrathin films, which was estimated by using electron energy loss spectroscopy, was between 60 and 80 nm.

**Conductivity Measurements.** The block copolypeptoid membranes with thicknesses of about 40 $\mu$m were obtained by methods described in the SAXS experimental section. In-plane proton conductivity of membranes equilibrated in humid air was measured in the same humidity chamber as that used in the water uptake measurements by ac impedance spectroscopy using platinum electrodes in the standard four-probe configuration using a BekkTech sample clamp. Data were collected over a frequency range of 1 Hz−100 kHz. The membrane was allowed to equilibrate at each humidity level for 24 h before a measurement was made. The conductivity, $\sigma$, is given by eq 4:

$$\sigma = l/(w \times h \times R) \quad (4)$$

where $w$ and $h$ are width and thickness of the membrane, respectively, $R$ is the touchdown of the Nyquist semicircle on the real axis, and $l$ is the distance between the inner platinum electrodes.

## ■ RESULTS AND DISCUSSION

The volume fraction of the phosphonate block (Npm) was varied from 0.13 to 0.44 in order to obtain a variety of nanoscale morphologies and thus probe the impact of morphology on conductivity. The Neh block, made from a racemic monomer, was chosen as the hydrophobic structural block and is known to be amorphous.[40] The structure of the synthesized block copolypeptoids is shown in Figure 1. Block

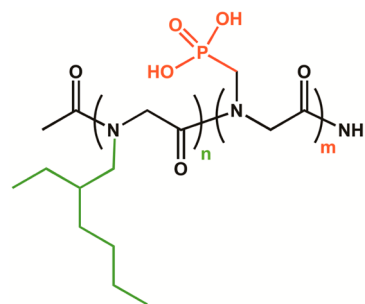molecular weights and purity characteristics are given in Table 1.



**Figure 1.** Structure of block copolypeptoid poly-*N*-(2-ethyl)hexyl-glycine-*block*-poly-*N*-phosphonomethylglycine, or pNeh$_n$-*b*-pNpm$_m$; $n$ and $m$ are the degrees of polymerization of pNeh (green) and pNpm (red) blocks, respectively.

**Table 1. Characteristics of the Block Copolypeptoid pNeh$_n$-*b*-pNpm$_m$ Synthesized**

| peptoids | $\phi_{Npm}$ | molar mass[a] (g/mol, calc/obs) | molar mass[b] (g/mol) | dispersity ($Đ$)[c] |
|---|---|---|---|---|
| pNeh$_9$-*b*-pNpm$_9$ | 0.44 | 2941.4/2941.4 | 2942.8 | 1.0003 |
| pNeh$_{18}$-*b*-pNpm$_{18}$ | 0.44 | 5823.8/5824.7 | | 1.0001 |
| pNeh$_{26}$-*b*-pNpm$_{10}$ | 0.23 | 5969.9/5970.9 | | 1.0001 |
| pNeh$_{30}$-*b*-pNpm$_6$ | 0.13 | 6042.5/6043.4 | | 1.0002 |

[a]As determined by ESI. [b]As determined by MALDI. [c]PDI is estimated based on the ESI and MALDI data as described in ref 40.

We first investigated the thermal properties of the block copolymers by TGA and DSC. TGA results show that degradation of the block copolypeptoids begins at 300 °C, indicating stability of the *N*-phosphonomethylglycine units (Figure S5). The lack of melting peaks and crystallization exotherms in DSC data (not shown) indicate that, as expected, all of the pNeh-*b*-pNpm copolymers are amorphous.

The water uptake properties of the phosphonated peptoid block copolymers are shown in Figure 2, where the number of water molecules per phosphonate group or hydration number, $\lambda$, is plotted as a function of the dry block copolymer volume fraction, $\phi_{Npm}$, at relative humidities (RH) of 50% and 98%. The volume fractions of the pNpm-rich microphases in the wet
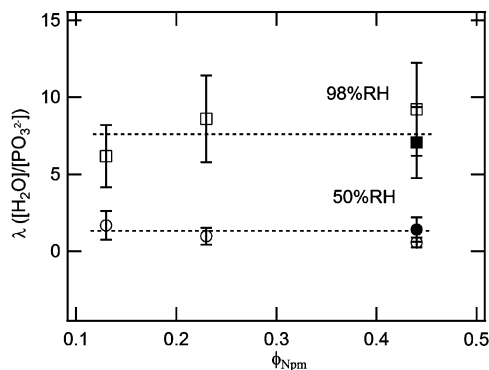


**Figure 2.** Plots of hydration number, $\lambda$, as a function of volume fraction of the Npm block ($\phi_{Npm}$), in the dry state at 25 °C. Circles: RH = 50%; squares: RH = 98%. Open symbols: $m + n = 36$. Filled symbols: $m + n = 18$. To a good approximation, hydration number is independent of block copolymer composition and chain length.

**Table 2. Characteristics of pNeh-*b*-pNpm Copolymers**[a]

| polypeptoids | $\phi_{Npm}$ | $\phi_{Npm,wet}$ (RH = 50%) | $\phi_{Npm,wet}$ (RH = 98%) | morphology (dry) | morphology (RH = 98%) (hydrated) | $d$ (nm) | $d_{wet}$ (nm) | $\lambda$ (RH = 98%) | conductivity (mS/cm) (RH = 98%) |
|---|---|---|---|---|---|---|---|---|---|
| pNeh$_9$-*b*-pNpm$_9$ | 0.44 | 0.46 | 0.60 | lamellar | hexagonal | 6.1 | 6.8 | 7.05 | 1.9 |
| pNeh$_{18}$-*b*-pNpm$_{18}$ | 0.44 | 0.48 | 0.63 | lamellar | lamellar | 10.3 | 11.9 | 9.22 | 8.1 |
| pNeh$_{26}$-*b*-pNpm$_{10}$ | 0.23 | 0.25 | 0.39 | lamellar | lamellar | 11.1 | 12.0 | 8.59 | 1.6 |
| pNeh$_{30}$-*b*-pNpm$_6$ | 0.13 | 0.16 | 0.22 | disordered lamellar | disordered lamellar | 8.2 | 8.6 | 6.17 | N/A |

[a] $d$ is the center-to-center distance between adjacent pNpm lamellae in the air. $d_{wet}$ is the center-to-center distance between adjacent pNpm lamellae at RH = 98%. $\phi_{Npm}$ is the volume fraction of the pNpm block in the air. $\phi_{Npm,wet}$ is the volume fraction of the pNpm block at RH = 98% and 50%. The data are assumed ideal mixing. N/A is not avaiable. $\lambda$ = water uptake (%) × 10/(MW$_{H_2O}$ × IEC).

state, $\phi_{Npm,wet}$, were determined from the water uptake measurements and known copolymer compositions, assuming perfect microphase separation and neglecting volume changes on mixing, and these values are given in Table 2. As seen in Figure 2, $\lambda$ is largely independent of block copolymer composition and chain length. The average value of $\lambda$ at RH = 98% is 7.8, while that at RH = 50% is 1.2. These values are substantially lower than those obtained in sulfonated block copolymers. Typical values of $\lambda$ at RH = 98% in sulfonated block copolymers is 13.[46]

The phase behavior of the pNeh-*b*-pNpm block copolymers in dry and hydrated states was studied by SAXS. We report data obtained from dry samples that were exposed to air (RH = 35%) and wet samples placed in a closed SAXS sample stage containing water. Lacking a better alternative, we assume that the SAXS data from the wet samples indicate the sample morphology at RH = 98% (the relative humidity at which proton conductivity and water uptake was measured). SAXS intensity is plotted as a function of the magnitude of the scattering vector, $q$, in Figure 3. Under dry conditions, most samples exhibit a primary peak at $q = q^*$ and a second-order peak at $q = 2q^*$, consistent with the presence of a lamellar phase. Additional higher order peaks at $q = 3q^*$, $4q^*$, and $5q^*$ are seen in some of the samples; these higher order peaks are also consistent with a lamellar phase. In all cases except pNeh$_{30}$-*b*-pNpm$_6$, the peaks are relatively sharp, indicating the presence of well-ordered lamellar morphologies. In contrast, the SAXS peaks of dry pNeh$_{30}$-*b*-pNpm$_6$ are broad, suggesting a disordered morphology. The primary peak of the pNeh$_{26}$-*b*-pNpm$_{10}$ sample has a high-$q$ shoulder that is absent in the higher order peaks. We do not know the reason for this observation. The observation of lamellar morphologies in this composition window is consistent with a previous study of amorphous peptoid diblock copolymers,[40] where we reported the formation of lamellar phases, irrespective of block copolymer composition. The characteristic length of the periodic structure, $d$, is given by $d = 2\pi/q^*$. The values of $d$ thus obtained are given in Table 2. At a fixed chain length of 36 ($m + n = 36$), $d$ decreases from 10.3 to 8.2 nm as $\phi_{Npm}$ decreases from 0.44 to 0.13, consistent with the classical theory on block copolymer self-assembly by Leibler.[47] Not surprisingly, $d$ is dependent on the chain length ($m + n$); at fixed $\phi_{Npm}$ = 0.44, $d$ decreases from 10.3 to 6.1 nm, as $m + n$ decreases from 36 to 18.

The morphology of dry pNeh-*b*-pNpm copolymers was also studied by dark field TEM as shown in Figure 4. It is important to note that our sample preparation approach, described in the Experimental Section, results in the self-assembly of morphologies in free-standing films with thicknesses between 60 and 80 nm. (Attempts to use a cryogenic microtome to obtain sections were not successful.) In a previous study, it was shown that
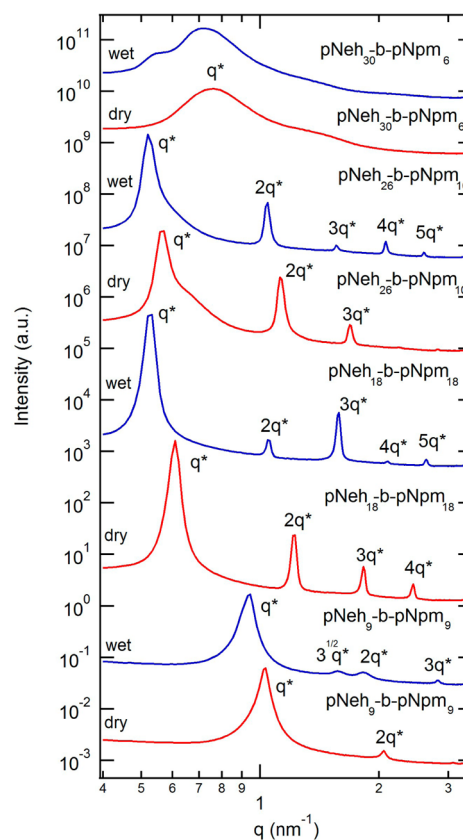


**Figure 3.** SAXS profiles at room temperatures for pNeh$_{18}$-*b*-pNpm$_{18}$, pNeh$_{26}$-*b*-pNpm$_{10}$, pNeh$_{30}$-*b*-pNpm$_6$, and pNeh$_9$-*b*-pNpm$_9$ in dry (red) and hydrated (blue) states.

free-standing films of this nature can exhibit morphologies that are similar but not identical to the bulk morphology.[48] In Figures 4a and 4b we show micrographs of pNeh$_9$-*b*-pNpm$_9$ and pNeh$_{18}$-*b*-pNpm$_{18}$. Lamellar microphases with poor long-range order are seen in pNeh$_9$-*b*-pNpm$_9$. A higher degree of long-range lamellar structure is seen in pNeh$_{18}$-*b*-pNpm$_{18}$. In contrast, the pNeh$_{26}$-*b*-pNpm$_{10}$ samples exhibited honeycomb morphologies by TEM (Figure 4c). Inside the honeycombs, pNeh$_{26}$-*b*-pNpm$_{10}$ exhibits lamellae arranged like an onion. The micrograph of pNeh$_{30}$-*b*-pNpm$_6$ (Figure 4d) has a similar lamellar structure to that of pNeh$_{18}$-*b*-pNpm$_{18}$. The lamellae seen in the micrographs of pNeh$_9$-*b*-pNpm$_9$, pNeh$_{18}$-*b*-pNpm$_{18}$, and pNeh$_{26}$-*b*-pNpm$_{10}$ are consistent with the distances observed by SAXS. In contrast, the lamellar structure inside the honeycombs in pNeh$_{30}$-*b*-pNpm$_6$ appears disordered, consistent with the broad SAXS primary peak seen in Figure 3.

Returning to the SAXS data (Figure 3), we see that the lamellar morphology is obtained in all the samples with $m + n =$
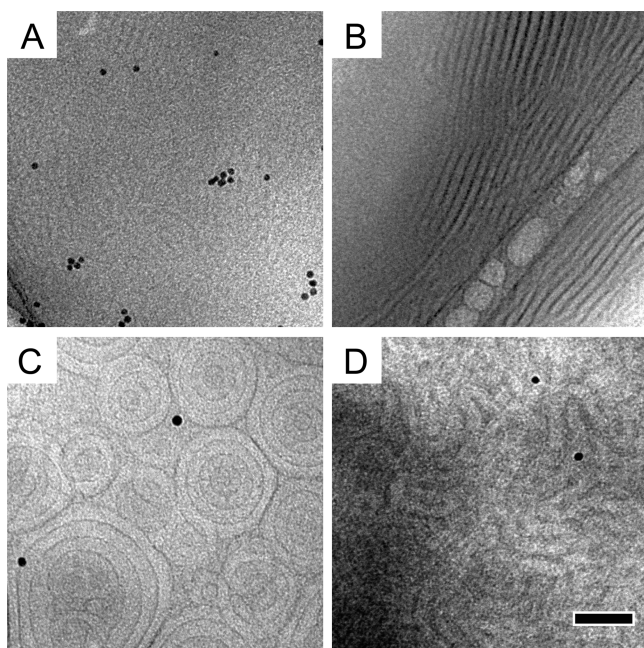
**Figure 4.** Energy filtered transmission electron microscopy (EFTEM) analysis indicates the various morphologies of the moisture annealed pNeh$_m$-$b$-pNpm$_n$ drop-casted thin films: (a) pNeh$_9$-$b$-pNpm$_9$, (b) pNeh$_{18}$-$b$-pNpm$_{18}$, (c) pNeh$_{26}$-$b$-pNpm$_{10}$, and (d) pNeh$_{30}$-$b$-pNpm$_6$. The dark microphases comprise phosphonated blocks (pNpm), the bright microphases comprise pNeh blocks, and the scale bar is 50 nm for all images. The dark circles represent gold nanoparticles ($\sim$5 nm) used as fiducial markers for TEM imaging.

36 in the wet state. The ordered morphologies in the wet state are generally better defined than in the dry state. For example, the higher order peaks at 4$q$* and 5$q$* are seen in the wet pNeh$_{26}$-$b$-pNpm$_{10}$ sample with $\phi_{\text{Npm}}$ = 0.23 but are absent in the dry state. The reduced intensity of the 2$q$* peak in the pNeh$_{18}$-$b$-pNpm$_{18}$ sample suggests that $\phi_{\text{Npm,wet}}$ must be in the vicinity of 0.5. This is consistent with estimates of $\phi_{\text{Npm,wet}}$ (Table 2). The SAXS patterns of pNeh$_{30}$-$b$-pNpm$_6$ in the dry and wet states are similar except for the low-$q$ shoulder that appears in the wet state. All primary peaks shift to a lower $q$* values in the wet state, indicating an increase in $d$ in wet state. Interestingly, in the wet pNeh$_9$-$b$-pNpm$_9$ sample ($m + n$ = 18) ($\phi_{\text{Npm,wet}}$ = 0.60), a primary peak at $q = q$* and higher order peaks at $q = \sqrt{3}q$*, 2$q$*, and 3$q$* are visible, indicating the presence of hexagonally packed cylinders. This is in contrast to what is typically observed in uncharged block copolymers: samples with symmetric composition (i.e., with the volume fraction of each block in the vicinity of 0.5) exhibit a lamellar morphology, in the dry state or when swollen with selective solvents.[47,49,50] The presence of a cylindrical morphology in hydrated pNeh$_9$-$b$-pNpm$_9$ is thus interesting. Such morphologies have been seen before in nearly symmetric sulfonated block copolymers[24] and are predicted by theories on charged block copolymers.[51,52] In these systems,[24,54,55] the charged block forms the matrix. We thus expect the matrix of wet pNeh$_9$-$b$-pNpm$_9$ to comprise hydrated pNpm, while the cylinders are expected to comprise dry pNeh chains. Another point worth noting is that the higher molecular weight sample with the same composition, pNeh$_{18}$-$b$-pNpm$_{18}$, exhibits a lamellar phase in the wet state. It is evident that the set of peptoid block copolymers used in this study present a wide variety of morphologies in the hydrated state.

The proton conductivity ($\sigma$) of the block copolymers equilibrated in humid air with RH = 98% was determined as a function of $\phi_{\text{Npm,wet}}$ (Figure 5). Note that the hydration
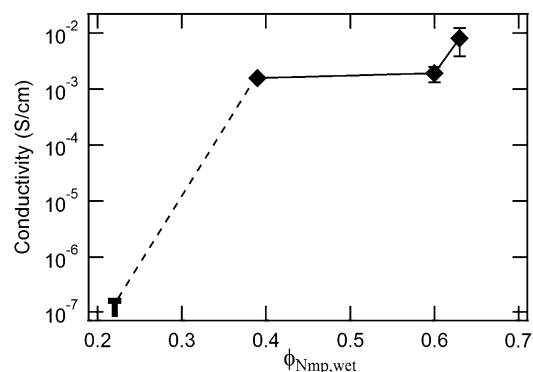


**Figure 5.** Proton conductivity plots of pNeh-$b$-pNpm as a function of $\phi_{\text{Npm,wet}}$ at RH = 98% and 25 °C. The conductivity of the sample with $\phi_{\text{Npm,wet}}$ = 0.22 was below the limit of detection and we thus can only provide an upper bound for the conductivity, $1.5 \times 10^{-7}$ S/cm.

number in all of the samples including pNeh$_{30}$-$b$-pNpm$_6$ were similar: $\lambda$ = 7.8 $\pm$ 1.4. The conductivity of hydrated pNeh$_{30}$-$b$-pNpm$_6$ was below the detection limit of our instrument (about $1.5 \times 10^{-7}$ S/cm). We can thus only provide an upper bound for the conductivity of this sample. The conductivities of the other samples were above $10^{-3}$ S/cm. The most conductive sample exhibits a proton conductivity of $8 \times 10^{-3}$ S/cm, a remarkably high value considering that $\lambda$ is only 9.2. It is likely that there are two possible reasons for the sharp increase in conductivity as $\phi_{\text{Npm,wet}}$ increases from 0.22 to 0.39: (1) the morphology of the ionic microphase undergoes a percolation transition, or (2) the mixing of pNeh segments in the pNpm-rich domains interferes with ion transport.

The conductivity of ordered block copolymers with one conducting block, $\sigma$, is often described by the equation[54−56]

$$\sigma = f\phi_c\sigma_c \tag{5}$$

where $f$ is the morphology factor related to geometry of the conducting phase, $\phi_c$ is the volume fraction of the conducting phase, and $\sigma_c$ is the intrinsic conductivity of the conducting phase. We assume that $\phi_c = \phi_{\text{Npm,wet}}$. In the case of pNeh$_{18}$-$b$-pNpm$_{18}$ and pNeh$_{26}$-$b$-pNpm$_{10}$, $f$ is 2/3 (lamellar conducting domains), while in the case of pNeh$_9$-$b$-pNpm$_9$, $f$ is 1 (conducting phase is the matrix of a hexagonally packed cylinder morphology). We take $\sigma_c$ of pNeh$_{30}$-$b$-pNpm$_6$ to be zero. The value of $\sigma_c$ corresponds to the estimated conductivity of hydrated pNpm domains with $\lambda$ = 8.1 $\pm$ 1.1; small differences in $\lambda$ between samples will be discussed shortly. To a good approximation, $\sigma_c$ is a linear function of $n$ (Figure 6). Similar trends have been observed in other charged block copolymers; the intrinsic conductivity of block copolymer domains increases with increasing chain length. One of the factors that contribute to this effect is segregation strength. As segregation strength increases, the microphases become more sharply defined; i.e., the concentration of nonconducting chains in the conducting domains decreases. One expects segregation strength to increase with increasing chain length at constant block copolymer composition. The data in Figure 6a are consistent with this expectation.

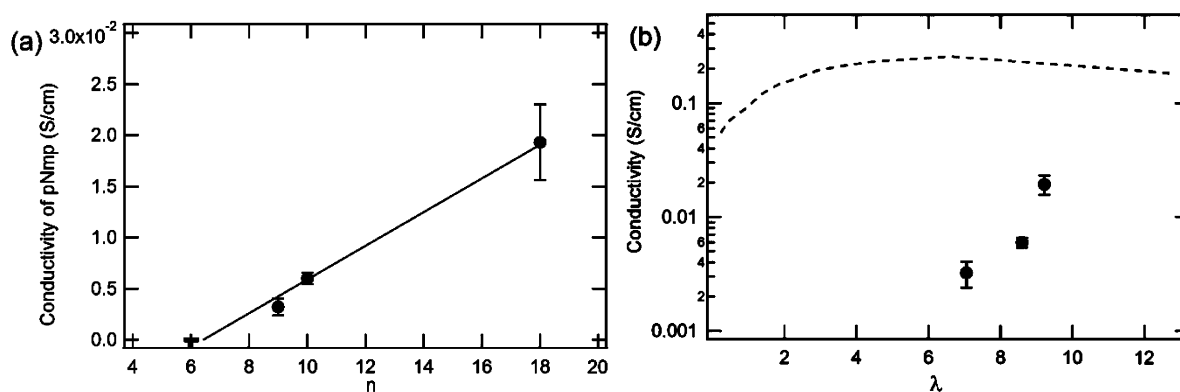In Figure 6b, we compare the intrinsic conductivity of the hydrated pNpm-rich domains in the block copolypeptoid, $\sigma_c$,

**Figure 6.** (a) Estimated conductivity of hydrated pNpm domains, $\sigma_c$, with hydration number, $\lambda = 8.1 \pm 1.1$, obtained from block copolymers equilibrated in humid air at 25 °C with RH = 98% as a function of the number of repeat units in each pNpm block, $n$. The solid line represents a linear fit. (b) $\sigma_c$ as a function of $\lambda$ (data of conducting samples in part a). The dashed curve represents the proton conductivity of aqueous $H_3PO_4$ as a function of $\lambda$, taken from ref 53.

with the conductivity of aqueous phosphoric acid ($H_3PO_4$) solutions at the same value of $\lambda$ taken from ref 53. The intrinsic conductivity of our copolymer with the highest conductivity (pNeh$_{18}$-$b$-pNpm$_{18}$) is about an order of magnitude lower than that of phosphoric acid. Since the conductivity of phosphoric acid solutions represents an upper limit for the intrinsic conductivity of hydrated microphases with phosphonic acid groups, the maximum attainable value of $\sigma_c$ is between 0.15 and 0.25 S/cm. It may thus be possible to improve the conductivity of phosphonated block copolymers by as much as an order of magnitude by increasing segregation strength or by designing other phosphonated polymers.

## CONCLUSION

A series of novel phosphonated diblock copolymers poly-$N$-(2-ethyl)hexylglycine-$block$-poly-$N$-phosphonomethylglycine (pNeh-$b$-pNpm) with dispersity ≤1.0003 were synthesized by solid-phase synthesis. The morphologies of the block copolypeptoids were determined by SAXS and TEM. In the dry state, the sample with $\phi_{Npm} = 0.13$ was disordered while others exhibited lamellar morphologies. In most cases, the morphologies of the dry and hydrated states were similar, except for pNeh$_9$-$b$-pNpm$_9$, which exhibited a cylindrical morphology in the hydrated state. The hydration numbers ($\lambda$) of the pNeh-$b$-pNpm membranes equilibrated in air with RH = 98% were comparable (was $8.1 \pm 1.1$ water molecules per phosphonate group), but proton conductivities were widely different. The disordered sample was an insulator (conductivity $<10^{-7}$ S/cm) while conductivities as high as 0.008 S/cm were obtained in the ordered samples. The estimated intrinsic conductivity of hydrated pNpm microphases increases linearly with the degree of polymerization of the pNpm block. The high molecular weight, symmetric pNeh-$b$-pNpm sample exhibited maximum conductivity.

The results of this study provide the basis for the design of proton-conducting phosphonated polymer electrolytes with higher conductivity. Peptoid block copolymers provide a novel platform for studying the relationship between molecular structure and transport. The ability of phosphonate-containing copolymers to conduct protons at low degrees of hydration makes them particularly attractive for electrochemical applications.

## ASSOCIATED CONTENT

**Ⓢ Supporting Information**

The Supporting Information is available free of charge on the ACS Publications website at DOI: 10.1021/acs.macromol.6b00353.

Figures S1−S6 (PDF)

## AUTHOR INFORMATION

**Corresponding Authors**

*E-mail rnzuckermann@lbl.gov (R.N.Z.).
*E-mail nbalsara@berkeley.edu (N.B.).

**Notes**

The authors declare no competing financial interest.

## ACKNOWLEDGMENTS

## REFERENCES

(1) Steele, B. C. H.; Heinzel, A. Materials for fuel-cell technologies. *Nature* **2001**, *414*, 345−352.
(2) Elabd, Y. A.; Hickner, M. A. Block Copolymers for Fuel Cells. *Macromolecules* **2011**, *44*, 1−11.
(3) Haggin, J. Inorganic hosts bind aromatic amino acids. *Chem. Eng. News* **1995**, *73*, 28−29.
(4) Srinivasan, S.; Ticianelli, E. A.; Derouin, C. R.; Redondo, A. Advances in solid polymer electrolyte fuel cell technology with low platinum loading electrodes. *J. Power Sources* **1988**, *22*, 359−375.
(5) Curtin, D. E.; Lousenberg, R. D.; Henry, T. J.; Tangeman, P. C.; Tisack, M. E. Advanced materials for improved PEMFC performance and life. *J. Power Sources* **2004**, *131*, 41−48.
(6) Yeo, S. C.; Eisenberg, A. Physical properties and supermolecular structure of perfluorinated ion-containing (nafion) polymers. *J. Appl. Polym. Sci.* **1977**, *21*, 875−898.

(7) Gierke, T. D.; Munn, G. E.; Wilson, F. C. The morphology in nafion perfluorinated membrane products, as determined by wide- and small-angle x-ray studies. *J. Polym. Sci., Polym. Phys. Ed.* **1981**, *19*, 1687−1704.

(8) Hsu, W. Y.; Gierke, T. D. Ion transport and clustering in nafion perfluorinated membranes. *J. Membr. Sci.* **1983**, *13*, 307−326.

(9) Xue, T.; Trent, J. S.; Osseo-Asare, K. Characterization of nafion® membranes by transmission electron microscopy. *J. Membr. Sci.* **1989**, *45*, 261−271.

(10) Zawodzinski, T. A.; Neeman, M.; Sillerud, L. O.; Gottesfeld, S. Determination of water diffusion coefficients in perfluorosulfonate ionomeric membranes. *J. Phys. Chem.* **1991**, *95*, 6040−6044.

(11) Zawodzinski, T. A.; Derouin, C.; Radzinski, S.; Sherman, R. J.; Smith, V. T.; Springer, T. E.; Gottesfeld, S. Water Uptake by and Transport Through Nafion® 117 Membranes. *J. Electrochem. Soc.* **1993**, *140*, 1041−1047.

(12) Zawodzinski, T. A.; Davey, J.; Valerio, J.; Gottesfeld, S. The water content dependence of electro-osmotic drag in proton-conducting polymer electrolytes. *Electrochim. Acta* **1995**, *40*, 297−302.

(13) Gebel, G. Structural evolution of water swollen perfluorosulfonated ionomers from dry membrane to solution. *Polymer* **2000**, *41*, 5829−5838.

(14) Elliott, J. A.; Hanna, S.; Elliott, A. M. S.; Cooley, G. E. Interpretation of the Small-Angle X-ray Scattering from Swollen and Oriented Perfluorinated Ionomer Membranes. *Macromolecules* **2000**, *33*, 4161−4171.

(15) James, P. J.; McMaster, T. J.; Newton, J. M.; Miles, M. J. In situ rehydration of perfluorosulphonate ion-exchange membrane studied by AFM. *Polymer* **2000**, *41*, 4223−4231.

(16) Haubold, H. G.; Vad, T.; Jungbluth, H.; Hiller, P. Nano structure of NAFION: a SAXS study. *Electrochim. Acta* **2001**, *46*, 1559−1563.

(17) Rubatat, L.; Gebel, G.; Diat, O. Fibrillar Structure of Nafion: Matching Fourier and Real Space Studies of Corresponding Films and Solutions. *Macromolecules* **2004**, *37*, 7772−7783.

(18) Kim, M.-H.; Glinka, C. J.; Grot, S. A.; Grot, W. G. SANS Study of the Effects of Water Vapor Sorption on the Nanoscale Structure of Perfluorinated Sulfonic Acid (NAFION) Membranes. *Macromolecules* **2006**, *39*, 4775−4787.

(19) Galperin, D. Y.; Khokhlov, A. R. Mesoscopic Morphology of Proton-Conducting Polyelectrolyte Membranes of Nafion® Type: A Self-Consistent Mean Field Simulation. *Macromol. Theory Simul.* **2006**, *15*, 137−146.

(20) Schmidt-Rohr, K.; Chen, Q. Parallel cylindrical water nano-channels in Nafion fuel-cell membranes. *Nat. Mater.* **2008**, *7*, 75−83.

(21) Kim, O.; Kim, S. Y.; Park, B.; Hwang, W.; Park, M. J. Factors Affecting Electromechanical Properties of Ionic Polymer Actuators Based on Ionic Liquid-Containing Sulfonated Block Copolymers. *Macromolecules* **2014**, *47*, 4357−4368.

(22) Kim, S. Y.; Yoon, E.; Joo, T.; Park, M. J. Morphology and Conductivity in Ionic Liquid Incorporated Sulfonated Block Copolymers. *Macromolecules* **2011**, *44*, 5289−5298.

(23) Yang, Y.; Shi, Z.; Holdcroft, S. Synthesis of Sulfonated Polysulfone-*block*-PVDF Copolymers: Enhancement of Proton Conductivity in Low Ion Exchange Capacity Membranes. *Macromolecules* **2004**, *37*, 1678−1681.

(24) Park, M. J.; Balsara, N. P. Phase Behavior of Symmetric Sulfonated Block Copolymers. *Macromolecules* **2008**, *41*, 3678−3687.

(25) Rubatat, L.; Shi, Z.; Diat, O.; Holdcroft, S.; Frisken, B. J. Structural Study of Proton-Conducting Fluorous Block Copolymer Membranes. *Macromolecules* **2006**, *39*, 720−730.

(26) Elabd, Y. A.; Napadensky, E.; Walker, C. W.; Winey, K. I. Transport Properties of Sulfonated Poly(styrene-b-isobutylene-b-styrene) Triblock Copolymers at High Ion-Exchange Capacities. *Macromolecules* **2006**, *39*, 399−407.

(27) Roziere, J.; Jones, D. J. Non-fluorinated polymer materials for proton exchange membrane fuel cells. *Annu. Rev. Mater. Res.* **2003**, *33*, 503−555.

(28) Depre, L.; Ingram, M.; Poinsignon, C.; Popall, M. Proton conducting sulfon/sulfonamide functionalized materials based on inorganic−organic matrices. *Electrochim. Acta* **2000**, *45*, 1377−1383.

(29) Samms, S. R.; Wasmus, S.; Savinell, R. F. Thermal Stability of Nafion® in Simulated Fuel Cell Environments. *J. Electrochem. Soc.* **1996**, *143*, 1498−1504.

(30) Kreuer, K. D. On the development of proton conducting polymer membranes for hydrogen and methanol fuel cells. *J. Membr. Sci.* **2001**, *185*, 29−39.

(31) Schuster, M. F. H.; Meyer, W. H. Anhydrous proton-conducting polymers. *Annu. Rev. Mater. Res.* **2003**, *33*, 233−261.

(32) Persson, J. C.; Jannasch, P. Intrinsically Proton-Conducting Benzimidazole Units Tethered to Polysiloxanes. *Macromolecules* **2005**, *38*, 3283−3289.

(33) Rusanov, A. L.; Kostoglodov, P. V.; Abadie, M. J. M.; Voytekunas, V. Y.; Likhachev, D. Y. Proton-conducting polymers and membranes carrying phosphonic acid groups. *Adv. Polym. Sci.* **2008**, *216*, 125−155.

(34) Rikukawa, M.; Sanui, K. Proton-conducting polymer electrolyte membranes based on hydrocarbon polymers. *Prog. Polym. Sci.* **2000**, *25*, 1463−1502.

(35) Lafitte, B.; Jannasch, P. On the prospects for phosphonated polymers as proton-exchange fuel cell membranes. *Adv. Fuel Cells* **2007**, *1*, 119−185.

(36) Sun, J.; Zuckermann, R. N. Peptoid Polymers: A Highly Designable Bioinspired Material. *ACS Nano* **2013**, *7*, 4715−4732.

(37) Simon, R. J.; Kania, R. S.; Zuckermann, R. N.; Huebner, V. D.; Jewell, D. A.; Banville, S.; Ng, S.; Wang, L.; Rosenberg, S.; Marlowe, C. K. Peptoids: a modular approach to drug discovery. *Proc. Natl. Acad. Sci. U. S. A.* **1992**, *89*, 9367−9371.

(38) Zuckermann, R. N.; Kerr, J. M.; Kent, S. B. H.; Moos, W. H. Efficient method for the preparation of peptoids [oligo(N-substituted glycines)] by submonomer solid-phase synthesis. *J. Am. Chem. Soc.* **1992**, *114*, 10646−10647.

(39) Tran, H.; Gael, S. L.; Connolly, M. D.; Zuckermann, R. N. Solid-phase submonomer synthesis of peptoid polymers and their self-assembly into highly-ordered nanosheets. *J. Visualized Exp.* **2011**, e3373.

(40) Sun, J.; Teran, A. A.; Liao, X.; Balsara, N. P.; Zuckermann, R. N. Nanoscale Phase Separation in Sequence-Defined Peptoid Diblock Copolymers. *J. Am. Chem. Soc.* **2013**, *135*, 14119−14124.

(41) Genet, J. P.; Uziel, J.; Port, M.; Touzin, A. M.; Roland, S.; Thorimbert, S.; Tanier, S. A practical synthesis of α-aminophosphonic acids. *Tetrahedron Lett.* **1992**, *33*, 77−80.

(42) Broeren, M. A. C.; de Waal, B. F. M.; van Genderen, M. H. P.; Sanders, H. M. H. F.; Fytas, G.; Meijer, E. W. Multicomponent Host−Guest Chemistry of Carboxylic Acid and Phosphonic Acid Based Guests with Dendritic Hosts: An NMR Study. *J. Am. Chem. Soc.* **2005**, *127*, 10334−10343.

(43) Sun, J.; Teran, A. A.; Liao, X.; Balsara, N. P.; Zuckermann, R. N. Crystallization in Sequence-Defined Peptoid Diblock Copolymers Induced by Microphase Separation. *J. Am. Chem. Soc.* **2014**, *136*, 2070−2077.

(44) Rosales, A. M.; McCulloch, B. L.; Zuckermann, R. N.; Segalman, R. A. Tunable Phase Behavior of Polystyrene-Polypeptoid Block Copolymers. *Macromolecules* **2012**, *45*, 6027−6035.

(45) Ilavsky, J. Nika: software for two-dimensional data reduction. *J. Appl. Crystallogr.* **2012**, *45*, 324−328.

(46) Xin, W.; Yakovlev, S.; Beers, K. M.; Park, M. J.; Mullin, S. A.; Downing, K. H.; Balsara, N. P. On the Origin of Slow Changes in Ionic Conductivity of Model Block Copolymer Electrolyte Membranes in Contact with Humid Air. *Macromolecules* **2010**, *43*, 5306−5314.

(47) Leibler, L. Theory of Microphase Separation in Block Copolymers. *Macromolecules* **1980**, *13*, 1602−1617.

(48) Yakovlev, S.; Wang, X.; Ercius, P.; Balsara, N. P.; Downing, K. H. Direct Imaging of Nanoscale Acidic Clusters in a Polymer Electrolyte Membrane. *J. Am. Chem. Soc.* **2011**, *133*, 20700−20703.

(49) Lodge, T. P.; Pudil, B.; Hanley, K. J. The Full Phase Behavior. For Block Copolymers In Solvents Of Varying Selectivity. *Macromolecules* **2002**, *35*, 4707−4717.

(50) Hanley, K. J.; Lodge, T. P.; Huang, C. *Macromolecules* **2000**, *33*, 5918−5931.

(51) Knychała, P.; Banaszak, M.; Park, M. J.; Balsara, N. P. Microphase Separation in Sulfonated Block Copolymers Studied by Monte Carlo Simulations. *Macromolecules* **2009**, *42*, 8925−8932.

(52) Gonzalez-Mozuelos, P.; de la Cruz, M. O. Random phase approximation for complex charged systems: Application to copolyelectrolytes (polyampholytes). *J. Chem. Phys.* **1994**, *100*, 507−517.

(53) Chin, D. T.; Chang, H. H. On the conductivity of phosphoric acid electrolyte. *J. Appl. Electrochem.* **1989**, *19*, 95−99.

(54) Shah, N.; Sax, J. E.; Ottino, J. M. Influence of morphology on the transport properties of polystyrene/polybutadiene blends: 2. Modelling results. *Polymer* **1985**, *26*, 1239−1246.

(55) Hallinan, D. T.; Balsara, N. P. Polymer Electrolytes. *Annu. Rev. Mater. Res.* **2013**, *43*, 503−525.

(56) Wieczorek, W.; Raducha, D.; Zalewska, A.; Stevens, J. R. Effect of Salt Concentration on the Conductivity of PEO-Based Composite Polymeric Electrolytes. *J. Phys. Chem. B* **1998**, *102*, 8725−8731.